Journal of Geophysical Research: Atmospheres

RESEARCH ARTICLE
10.1029/2017JD028019

Key Points:
- Long-lasting low wind speed conditions reduced wind power generation in the United States in 2015
- Retrospective climate predictions confirm that anomalous SSTs in the tropical Pacific Ocean forced the event

Supporting Information:
- Supporting Information S1

Correspondence to:
L. Lledó,
lledo@bsc.es

Citation:
Lledó, L., Bellprat, O., Doblas-Reyes, F. J., & Soret, A. (2018). Investigating the effects of Pacific sea surface temperatures on the wind drought of 2015 over the United States. *Journal of Geophysical Research: Atmospheres*, *123*, 4837–4849. https://doi.org/10.1029/2017JD028019

Received 10 NOV 2017
Accepted 9 APR 2018
Accepted article online 19 APR 2018
Published online 17 MAY 2018

Investigating the Effects of Pacific Sea Surface Temperatures on the Wind Drought of 2015 Over the United States

Llorenç Lledó[1], Omar Bellprat[1], Francisco J. Doblas-Reyes[1,2], and Albert Soret[1]

[1]Barcelona Supercomputing Center, Barcelona, Spain, [2]ICREA, Pg. Lluís Companys 23, Barcelona, Spain

Abstract During the first quarter of 2015 the United States experienced a widespread and extended episode of low surface wind speeds. This episode had a strong impact on wind power generation. Some wind farms did not generate enough cash for their steady payments, and the value of some assets decreased. Although the wind industry expressed their concerns, the episode has not received much attention from the scientific community and remains weakly understood. In this paper we aim to fill this gap and advance understanding of the underlying processes at seasonal time scales. Using retrospective climate predictions, we find that high sea surface temperatures in the western tropical Pacific ocean associated with a strongly positive phase of the North Pacific Mode played a central role to establish and maintain those wind anomalies. In a more general way it has also been shown that interannual variability of wind speed over North America is not only dominated by El Niño/Southern Oscillation but also by other sea surface temperature variations in the tropical Pacific. This new knowledge can be useful for industry stakeholders to anticipate future periods of low wind speed.

1. Introduction

In order to try to limit the effects of climate change and reduce greenhouse gas emissions, a huge effort to decarbonize the energy sector is taking place in many countries all over the world. One of the pillars of this decarbonization is the adoption of renewable energies. Wind energy, in particular, is the technology that has experienced the biggest growth in recent years (Global Wind Energy Council, 2016). However, wind farm owners, operators, and project developers face the challenge of understanding variability of wind speeds at several time scales to run their business successfully. In the forthcoming years renewables will reach high penetration levels in the electricity mix (Obama, 2017). Then transmission system operators will also need to understand weather and climate oscillations that impact electricity generation in order to guarantee energy supply and dimension transmission and backup facilities.

All these stakeholders are exposed to the risks that extreme events can bring. One of such events happened in 2015 in the United States, where wind power covers approximately 5% of the total electricity demand (U.S. Energy Information Administration, 2017). During the first quarter of 2015 (January–March), surface wind speeds were well below normal in most of the contiguous United States (see Figure 1), which reduced substantially the electricity generation of most of the wind farms in the country (U.S. Energy Information Administration, 2017). The wind speed reduction was especially relevant in Texas, Oklahoma, and Kansas, where most of the biggest wind farms are concentrated. The standardized anomalies reached values of more than three standard deviations away from the 1979–2014 mean in a widespread region, revealing that this was a very infrequent event. Indeed, the wind industry did not anticipate such low wind episode. Some companies experienced financial problems due to the lack of energy production and revenues (Meyer, 2015), and there were concerns on the value of the assets. The term "wind drought" was coined, and a lot of questions arose: When would winds revert back to normal conditions? Did anthropogenic climate change have an influence on this episode? Could this episode repeat in the near future (Brower, 2015; Maverick, 2015)?

All these questions direct us to ask what caused the episode. Some informal sources argued that the event was caused by a developing El Niño/Southern Oscillation (ENSO) warm phase, which is known to reduce winter and spring wind speeds in North America (Brower, 2015; ESS-BSC Catalogue, Earth System Services, Earth Science Department, Barcelona Supercomputing Center, 2016; St. George & Wolfe, 2009). However, El Niño was only weakly expressed at the time. The confusion might have derived from alarmist interpretations of seasonal forecasts, which anticipated a strong El Niño few months before (Climate Prediction Center and International

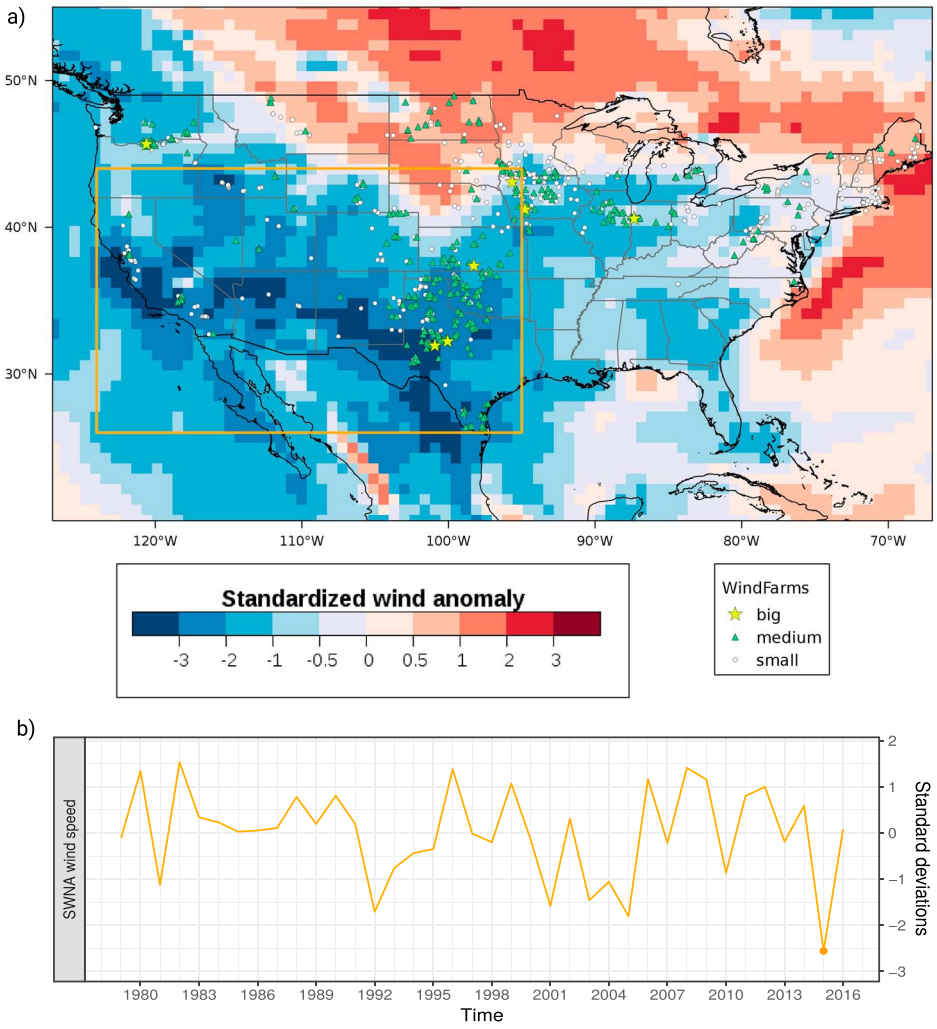

Figure 1. (a) Surface wind speed anomalies for the first quarter of 2015, expressed as the number of standard deviations away from the 1979–2014 mean for the same quarter. Values are from ERA-Interim reanalysis. The orange box delimits the region where the anomalies were more extreme (southwestern North America region, hereafter referred to as SWNA, 124°W–95°W and 26°N–44°N). The distribution of the U.S. wind farm fleet is overplotted: white dots, green triangles, and yellow stars represent small (<100 MW), medium (<400 MW), and big (>400 MW) wind farms (source: U.S. Energy Information Administration, 2016). (b) Temporal evolution of January–March mean wind speed anomalies over SWNA. 2015 is signaled with a dot. ERA = European Centre for Medium-Range Weather Forecasts Re-Analysis.

Research Institute for Climate and Society, 2014). Instead, the North Pacific Mode (NPM; Deser & Blackmon, 1995; Hartmann, 2014) was in a strongly positive phase during the event, as will be seen in section 3. The impact that NPM has on North American winter temperatures has already been studied by Hartmann (2014) and Bellprat et al. (2016) for extremely cold events. Seager et al. (2015) also related it to Californian drought in 2011–2014. In this study we analyze the role it could have played on stilling the wind in North America.

The positive phase of NPM, with high sea surface temperatures (SSTs) off the North American west coast and also in the western tropical Pacific, is thought to be favored by atmospheric variability known as North Pacific Oscillation (Baxter & Nigam, 2015; Ding et al., 2015). Alexander et al. (2010) showed how extratropical SST anomalies associated to NPM can propagate southwesterly due to the wind evaporation-SST feedback and persist on tropical Pacific waters until next winter. This teleconnection, first described by Vimont et al. (2003) and known as seasonal footprinting mechanism (SFM), explains why positive phases of NPM can trigger positive ENSO events the next winter (Di Lorenzo et al., 2010; Ding et al., 2015; Yu & Paek, 2015). However, Bond et al. (2015) already suggested that NPM impacts in North America might derive from tropical origin and not from the blob in North American shores. Indeed Stuecker (2018) very recently proved that Central Pacific

El Niño events (which are related to the tropical component of NPM) can produce in turn extratropical SST anomalies off the North America west coast. Here we will show the tropical roots of the wind drought episode by performing retrospective climate predictions with an atmosphere-only climate model where the role of SST patterns can be studied systematically.

The data sets, methods and characteristics of the atmospheric climate model used are described in section 2. In section 3 the event is analyzed. The coincidental state of the ocean during similar periods of low wind speed in the region is studied, and the role of ENSO and NPM in shaping the interannual variability of wind speed in North America is investigated. A set of sensitivity experiments using an Atmospheric General Circulation Model (AGCM) are presented in section 4. Discussion and concluding remarks follow in section 5.

2. Data and Methods

The January–March 2015 event has been analyzed using surface wind speed and SST anomalies in the European Centre for Medium-Range Weather Forecasts (ECMWF) Re-Analysis (ERA)-Interim reanalysis computed at monthly and 3-monthly time scales. ERA-Interim (Dee et al., 2011) is routinely produced at the ECMWF and provides gridded data at a spatial resolution of around 80 km (spectral resolution of T255). It is widely used in the wind industry to track anomalies. All the anomalies have been computed with respect to the 1979–2014 period, which is the period that was available when the event occurred. Moreover, the anomalies have been standardized dividing the absolute deviations by the standard deviation of the historical reference period. This helps to understand how extreme the anomalies were with respect to natural variability in the recent past.

Additionally, empirical orthogonal function analysis (EOF) and linear correlations have been employed to uncover relationships between SSTs and winds in the ERA-Interim data set. In order to achieve the largest possible sample size, the full ERA-Interim period 1979–2016 including the event was considered. The EOF patterns are normalized to 1, and the principal components (PC) have been standardized in the plots. The separation of EOF patterns has been tested with the North et al. rule of thumb (North et al., 1982; Wilks, 2005) using $n = 30$. Statistical significance for all correlations has been tested using a two-tailed t test with a confidence level of 95%.

The EC-Earth Earth-system model has been used for the AGCM experiments. EC-Earth is built using three main model components: Integrated Forecasting System for the atmosphere, Nucleus for European Modelling of the Ocean for the ocean, and Louvain-la-Neuve Sea Ice Model for the sea ice (Hazeleger et al., 2012, Prodhomme, Batté, et al., 2016). But in the present study only the atmospheric component (Integrated Forecasting System; cycle 36r) has been used, while sea ice and sea surface temperatures have been prescribed from ERA-Interim reanalysis on a daily basis. In all the experiments the spectral resolution of the atmospheric model is T255 (the same as ERA-Interim and corresponding to around 80 km) with a vertical resolution of 91 levels. For each of the experiments, a large ensemble with 100 members has been simulated. The singular vector perturbation technique (Buizza & Palmer, 1995) has been applied to the ERA-Interim observations to obtain slightly different but equally plausible initial conditions that result in diverging answers after the first few days of integrations. Then 3 months of simulations initialized on 1 January have been computed to cover the period of interest. The Autosubmit workflow manager (Manubens-Gil et al., 2016) has been used to manage efficiently the high number of simulations that were run. As AGCMs have systematic errors, a hindcast simulation for the period 1981–2010 has been prepared with 10 ensemble members to adjust the model biases. In order to identify and adjust those biases, we have followed the simple bias correction methodology described in Torralba et al. (2017), with separate adjustments for each month. This method adjusts both the bias and variance but does not inflate ensemble spread.

3. Anatomy of the Event

An analysis of the status of the ocean and atmosphere during the first quarter of 2015 (January–March, referred to as Q1) has been done to illustrate the particularities of the event. However, trying to understand cause-effect relationships from simultaneous anomalies in one event would be adventurous, and therefore similar patterns in the past records have been explored using two EOF analyses of wind speeds and SSTs from ERA-Interim reanalysis (Dee et al., 2011).

Figure 2 shows the evolution of SST and surface wind speed during Q1 2015 over the tropical and north Pacific Ocean and the United States. In the first column, a band of anomalously high SST can be seen off the

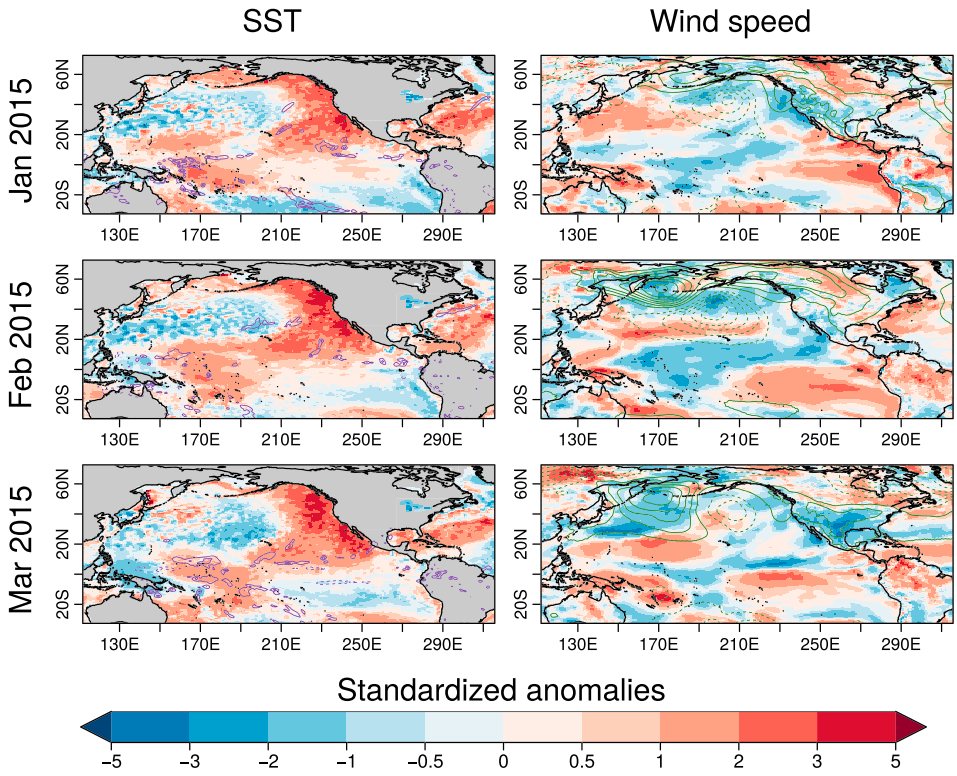

Figure 2. SST and surface wind speed anomalies for the first months of 2015, expressed as the number of standard deviations away from the 1979–2014 mean for the same month, drawn from ERA-Interim reanalysis. Purple contours show precipitation anomalies, and green contours show sea level pressure anomalies. Contour intervals are 5 mm/day and 2 hPa, respectively, with zero contour omitted. SST = sea surface temperature; ERA = European Centre for Medium-Range Weather Forecasts Re-Analysis.

western coast of North America. The western tropical Pacific also experienced remarkable positive anomalies, although not so outstanding in terms of standardized values. Those SST patterns resemble very much the anomalies associated to the positive phase of NPM (Hartmann, 2014). January and March are the months that experienced the highest wind anomalies of the period in the United States, in consistence with higher sea level pressures in the continent.

At the same time, during Q1 2015 the Arctic Oscillation (AO) was in a high phase (reaching 1.8 in March). Chen et al. (2013) showed how the AO in spring is a determinant for the SFM to be able to trigger an El Niño event next year. Interestingly, this event was followed by a strong El Niño next winter, so probably the SFM was very active during 2015.

Notice that the wind drought persisted also during the second quarter of the year (April–June) (see supporting information Figure S1), although here we will focus only on Q1. The region where the anomalies were higher during this period has been identified (see the orange box in Figure 1). We will refer to this region as southwestern North America region (SWNA, 124°W–95°W and 26°N–44°N).

To characterize the event with respect to past variability, an EOF analysis of Q1 surface winds over the United States (covering 140°W–65°W and 22°N–50°N and removing all water grid points) has been computed (see Figure 3). The first and second modes (referred to as m1 and m2 hereafter) account only for a 53% of the total variance in the EOF domain. But they correlate to 0.82 and 0.53 with the SWNA-averaged anomalies (presented in Figure 1b). Therefore, those two modes alone can reproduce a 95% of SWNA averaged anomalies. Hence, the Q1 2015 event can be decomposed into a slightly negative phase of the first mode and a strongly negative phase of the second mode (right column of Figure 3). Indeed, the second mode reached an outstanding absolute minimum in the records. This decomposition shows that the Q1 2015 anomaly is outstanding in terms of magnitude, but similar m2-shaped anomaly patterns were observed in the past, although not so strong. Analyzing those similar episodes in the historical records will help to better understand

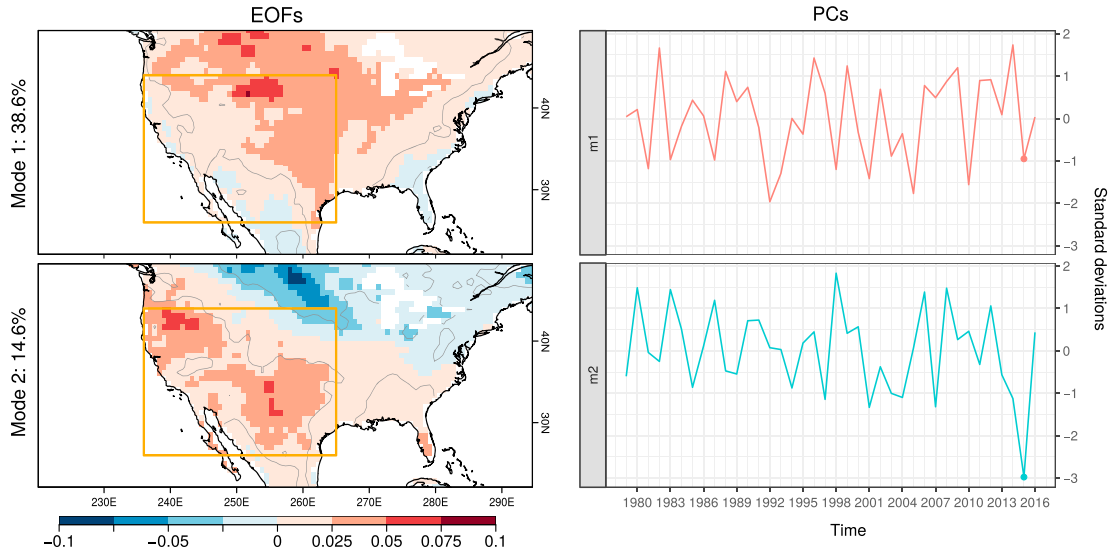

Figure 3. EOF analysis of Q1-averaged surface winds over the United States. (left column) EOF patterns. Gray contours enclose statistically significant areas. The orange box delimits the SWNA region. (right column) evolution of the normalized PCs. A dot highlights 2015 value in each time series. EOF = empirical orthogonal function; SWNA = southwestern North America region; PC = principal components.

the underlying processes. First m1 variability will be studied. Although m1 was not in a very high phase during the event, the description of the physical processes behind m1 variations, which are well known, will help to understand the processes behind m2 variability later.

Figure 4 shows the correlation coefficients between each of the two PCs and Q1 SSTs for all grid points. This plot identifies oceanic regions that could be contributing to generate those anomalies. For the first mode the pattern resembles very much the typical ENSO SST anomalies, in both the tropics and extratropics. We hypothesize that ENSO-like variations in the tropical Pacific have an influence on the strength of the first mode of U.S. wind speed. The sign of the correlations indicates that positive (warm) phases of ENSO are coincidental with negative phases of the first mode, that is, reduced wind speeds in most of the continent but specially in the north and center. For some time now, ENSO has been known to modify the general circulation patterns (Horel & Wallace, 1981) and to impart extratropical SST anomalies in both north and south Pacific oceans through the atmospheric bridge process (Alexander et al., 2002), specially during boreal winter

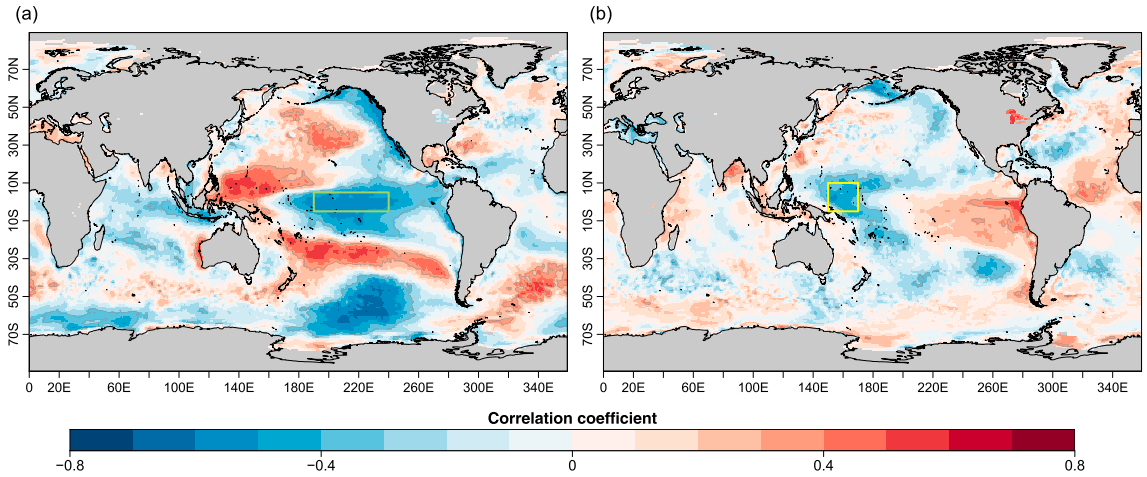

Figure 4. Correlation coefficients between Q1-averaged SSTs and the first PCs of U.S. wind speed. (a) Correlation with first mode. (b) Correlation with second mode. Two regions with high correlations are identified: the NINO3.4 region (green box, 170°W–120°W and 5°S–5°N, referred to as NINO3.4) and a western tropical Pacific region (yellow box, 150°E–170°E and 5°S–10°N, referred to as WTP). Gray contours enclose statistically significant areas. SST = sea surface temperature; PC = principal components.

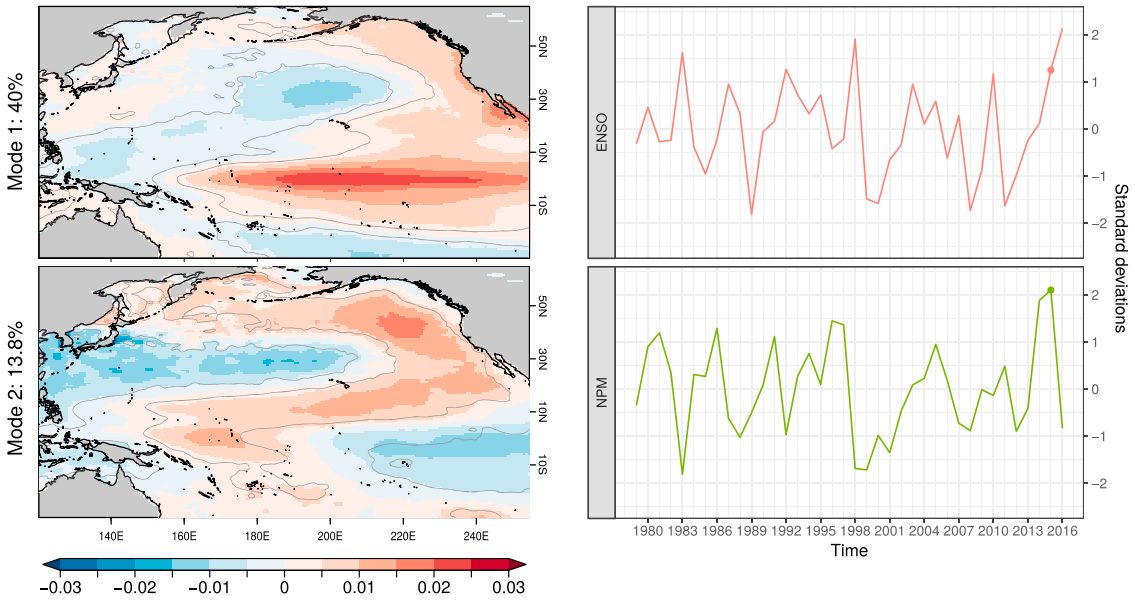

Figure 5. EOF analysis of Q1 Pacific SST. (left column) EOF patterns are drawn with color. Gray contours enclose statistically significant areas. (right column) Evolution of the normalized PCs. A dot highlights 2015 value in each time series. EOF = empirical orthogonal function; SST = sea surface temperature; PC = principal components.

and spring. Tropical SSTs are known to force midlatitudinal atmospheric circulation through warm anomalies that induce convective systems. The tropical convective motion results in midtropospheric diabatic heating and upper troposphere divergence that exert a quasi-stationary Rossby wave response and modulate the extratropical circulation (DeWeaver & Nigam, 2002; Trenberth et al., 1998). Extratropical SSTs in turn are mainly forced by wind speed variations which dominate underlying SSTs through evaporative processes: higher winds increase evaporation and reduce SSTs (Cayan, 1992). Therefore, it is plausible that whenever the atmospheric bridge is in place both extratropical SST and wind anomalies originate from tropical SST variations. With this in mind the NINO3.4 region (170°W–120°W and 5°S–5°N) has been highlighted in the map as an adequate indicator for the first mode of U.S. winds, even if higher correlations can be seen in the

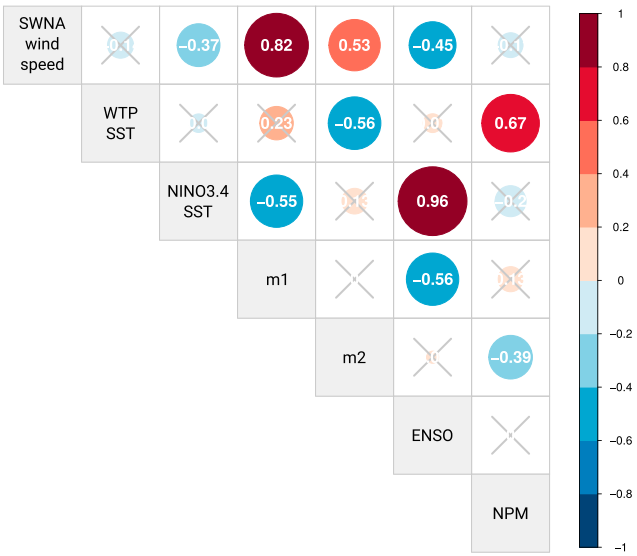

Figure 6. Linear correlation matrix including Q1 values of wind and SST anomalies and the first PCs of the two EOF analyses. A cross indicates nonsignificance at the 5% level. All the correlations can be found in the column above the corresponding label or in the row on its right. SST = sea surface temperature; PC = principal components; EOF = empirical orthogonal function.

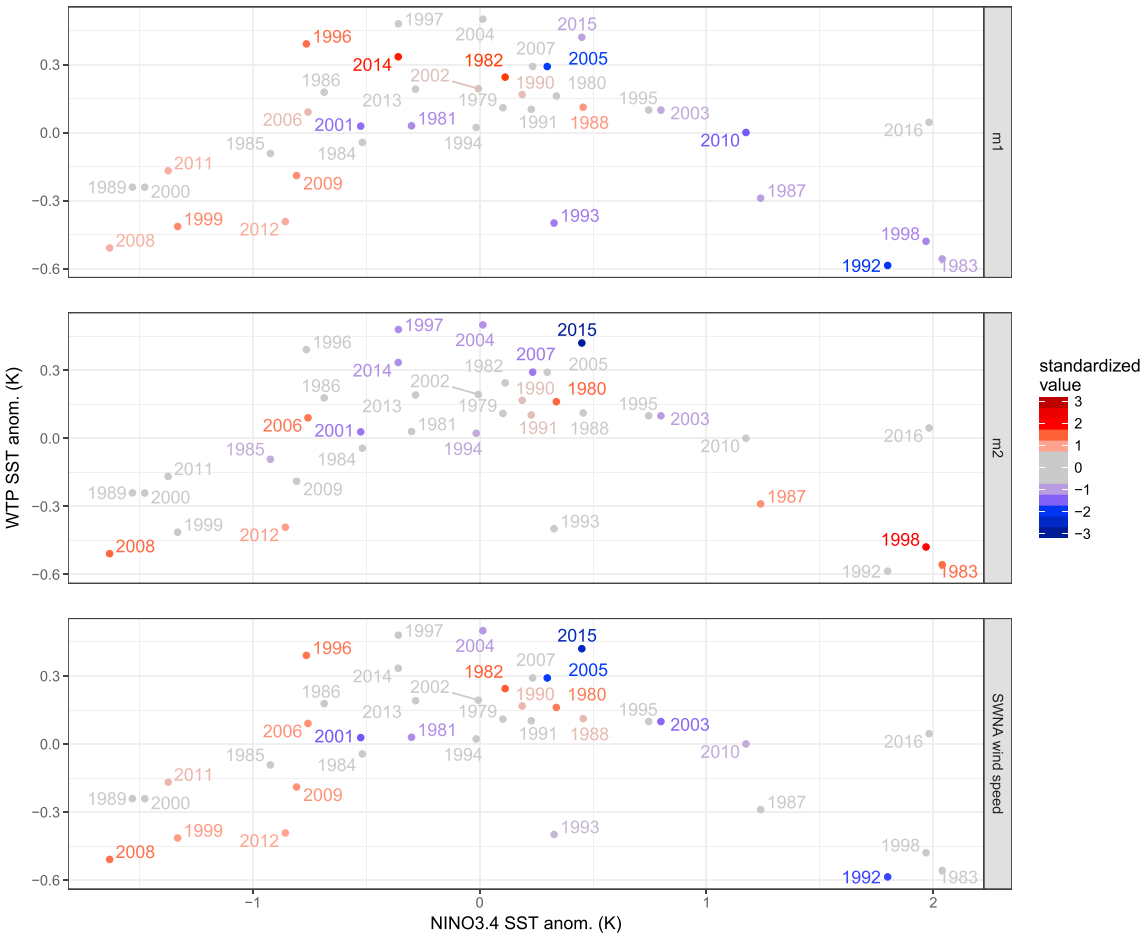

Figure 7. Scatterplot of NINO3.4 and WTP SSTs, labeled with the corresponding year and colored with standardized values of m1, m2, and SWNA wind speed in each of the panels. A strong nonlinear relationship between NINO3.4 and WTP SSTs can be seen. SST = sea surface temperature; SWNA = southwestern North America region; WTP = western tropical Pacific region.

southern Pacific ocean. A statistically significant correlation coefficient of −0.55 is obtained between Q1 NINO3.4 average SSTs and the first PC (see Figure 6).

For the second mode correlations are more modest (Figure 4b), but still two spots with moderate correlation can be identified: a region in the Western Tropical Pacific (150°E–170°E and 5°S–10°N, referred to as WTP), and another region of opposed sign in the eastern tropical Pacific. There are also spots with significance in the extratropics. A correlation of −0.56 is obtained between WTP SSTs and the second PC, suggesting that an atmospheric bridge teleconnection might be at play also in this case. The precipitation anomalies for Q1 2015 (see Figure 2) show enhanced convection in the western tropical Pacific and support this hypothesis for the 2015 event. This will be investigated further in section 4.

In order to better interpret the correlation map for the second mode, an EOF analysis of SSTs over tropical and north Pacific has been performed. The region has been set to 30°S–65°N and 120°E–105°W, following Hartmann (2014). Q1 averages for the 1979–2016 period have been employed, and the linear trend has been removed prior to analysis. Both the EOF patterns and the PC evolutions of the first two modes are shown in Figure 5. The third and fourth modes, although not relevant for the 2015 event, are shown in supporting information Figure S2. The first mode is ENSO, the dominant oscillation of global SSTs (Trenberth, 1997). The second mode corresponds to the NPM. A 1-year-lagged correlation coefficient of 0.57 between NPM and ENSO confirms it (not shown), as NPM is known to be one of the precursors of ENSO with 1 year of advance (Pegion & Alexander, 2013; Vimont et al., 2003; Wang et al., 2012). The Pacific Decadal Oscillation (Mantua et al., 1997), which is the second mode in Hartmann (2014), appears as the third mode in this decomposition.

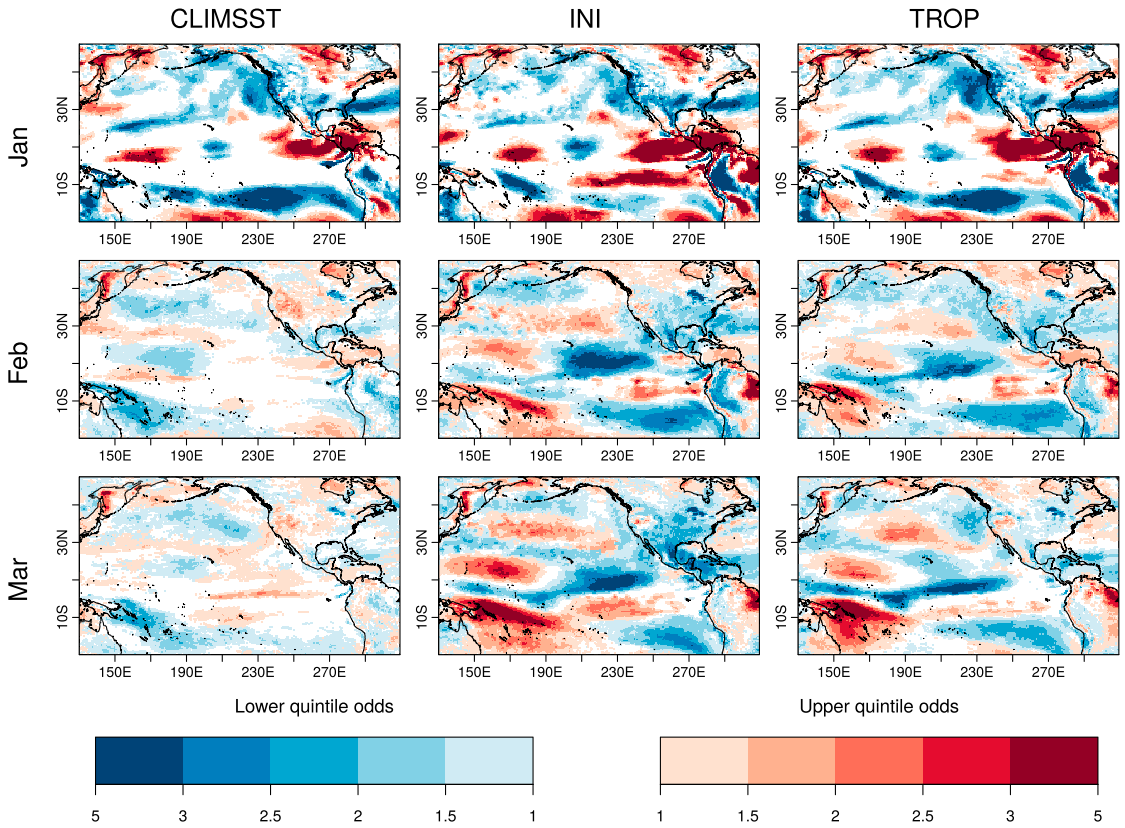

Figure 8. Odds of upper and lower quintiles of wind speed for CLIMSST (left column), INI (middle column), and TROP (right column) simulations initialized in January, for each of the three months. The odds are the ratio between the probability for the anomalies to be in the lower quintile, the interquintile range, or the upper quintile and the climatological probability of these three categories (20%, 60%, and 20%, respectively). Each grid point is colored with the category corresponding to the highest odds ratio. If the point corresponds to the interquintile range, the point is drawn in white. If the point is attributed to the lower (upper) quintile category, the corresponding odds ratio is plotted in blue (red). In January the impact of the initialization dominates the signal. In February and March the impact of different SST forcings emerges. SST = sea surface temperature.

Correlating the two U.S. wind speed PCs (m1 and m2) to the two Pacific SST PCs (ENSO and NPM), some linear relationships have been identified. Figure 6 summarizes the results in a matrix style plot. As pointed before, m1 anticorrelates with ENSO (−0.56). The m1 has also a weak positive correlation with NPM, but it is nonsignificant at 5% level. On the other hand, m2 has a significant correlation with NPM (−0.39), so that positive phases of NPM, with high SSTs in the WTP region, are related to reduced wind speeds in SWNA region, specially along the diagonal of the SWNA box. Notice that the NPM does not represent all SST variability in WTP region (see supporting information Text S1). This explains why the pattern in Figure 4b) does not match the NPM mode. Summarizing, in the past records there is a correspondence between ENSO (or NINO3.4 SSTs) and m1 events (31% of explained variance), and another correspondence between WTP SSTs (of which a portion is due to NPM) and m2 (also 31% of explained variance). From this we conclude that interannual variability of Q1 wind speed in North America is linked to NINO3.4 and WTP SST anomalies, that is, to ENSO, NPM, and any other SST variability in the WTP region.

Going back to the event under study, remember that Q1 2015 was marked by a strong negative phase of the second PC of U.S. wind speed and a slight negative phase of the first mode. Based on the PCs from EOF analysis of SST (Figure 5), during 2015 NPM was strongly positive, while ENSO was in a slightly positive phase, in accordance to the aforementioned relationships. This confirms that ENSO did not play a role in the episode, while NPM might play an important role.

In the previous paragraphs, the impact of NINO3.4 and WTP SSTs on North American wind speed has been undertaken separately. Analyzing it jointly will give a more detailed picture. Although NINO3.4 and WTP SSTs do not correlate significantly, a scatterplot (Figure 7) reveals that there is indeed a well-defined but nonlinear relationship between those SSTs, which results from ENSO nonlinearities and the antisymmetry of El Niño

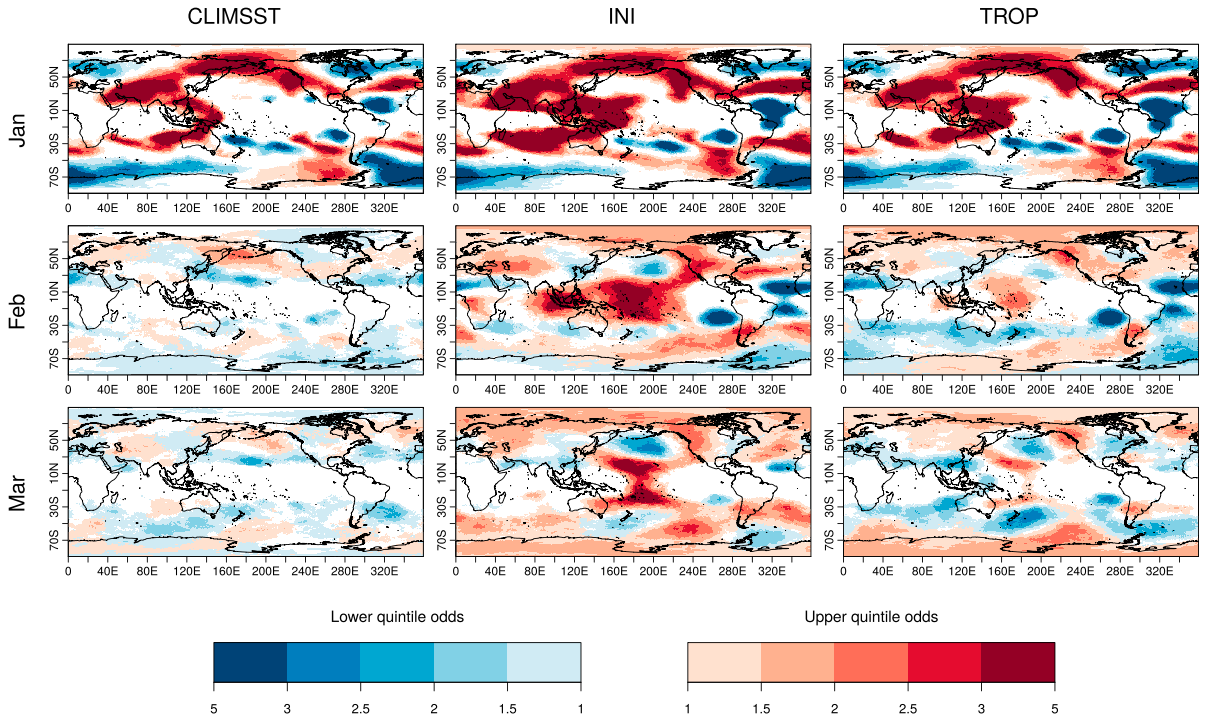

Figure 9. Same as Figure 8 but for geopotential height at 200 hPa. The Gill-type response can be seen in the INI and TROP simulations over the western Pacific. Its associated Rossby wave reaches North America.

and La Niña patterns (Monahan & Dai, 2004). Both highest and lowest NINO3.4 SSTs (i.e., strong ENSO phases) match low SSTs in WTP, with high WTP SSTs being observed only under relatively neutral ENSO conditions. Therefore, 2015-like anomalies might occur only under near-neutral ENSO states(see 1997, 2004, and 2007 in the top center of the panels). Regarding strong ENSO phases, in the first panel we see how m1 standardized value decreases from left to right, but in the second panel, m2 decreases from bottom to top. This implies that during strongly positive ENSO phases, m1 and m2 effects might compensate and moderate anomalies in SWNA (see, for instance, the strong 1983 or 1998 El Niño events on the bottom right of the panels), while under strongly negative ENSO phases m1 and m2 will contribute together to positive SWNA speed anomalies (e.g., 2008 on the bottom left).

4. Retrospective Model Predictions

To disentangle and confirm the relationships between NPM status and wind anomalies during the 2015 event uncovered in the previous section, a set of experiments using retrospective predictions with the EC-Earth forecast system have been performed (see section 2 for details). The January–March period has been simulated with different configurations, all initialized on 1 January 2015 using actual atmospheric conditions as initial conditions. The first model configuration uses January–March 2015 ERA-Interim daily SSTs as boundary conditions (referred to as INI hereafter). A second configuration uses a fixed SST climatology for January, February, and March (1981–2010) instead, to evaluate the impact of SST conditions in Q1 2015 (referred to as CLIMSST). Finally, a third simulation uses actual SST conditions only in the tropics (between 10°S and 10°N), climatological conditions north/south of 15°N/S and a transition zone in between (referred to as TROP).

Analyzing differences in the ensemble mean is not a good idea, because it is a deterministic metric and sometimes does not reflect the behavior of the distribution extremes. Instead, following Prodhomme, Doblas-Reyes, et al., (2016) we plot the odds of the INI, TROP, and CLIMSST simulations for higher and lower quintiles of wind speed (Figure 8). The probabilities for the anomalies to be in the lower quintile, the interquintile range, or the upper quintile are computed and then divided by the climatological probability of these three categories (20%, 60%, and 20%, respectively). These ratios are the odds: an odd higher than 1 indicates increased probabilities of the category. Then each grid point is colored with the category corresponding to the highest odds ratio. If the point corresponds to the interquintile range, the point is drawn in white.

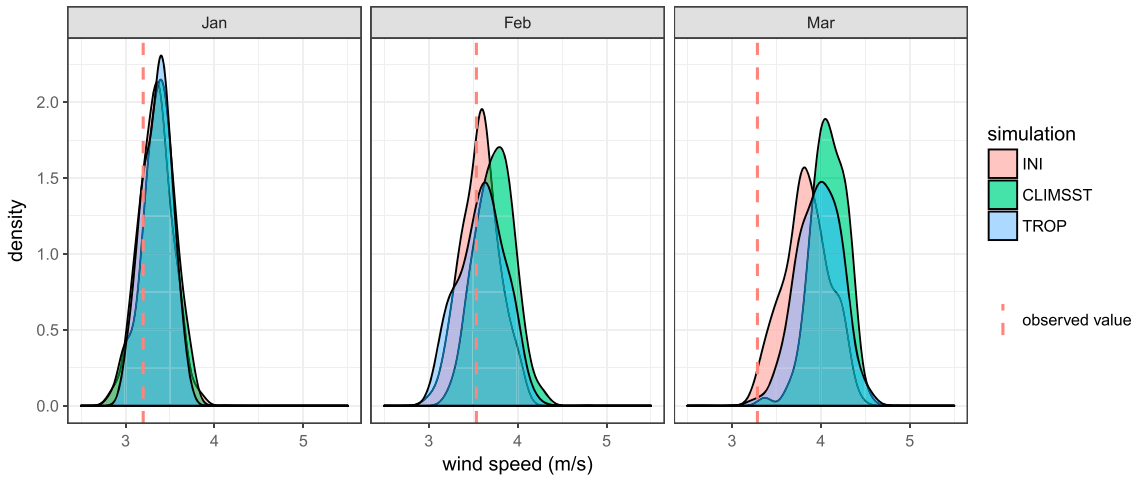

Figure 10. Probability distribution of SWNA wind speed for CLIMSST, INI and TROP simulations for January, February, and March. Dashed line indicates ERA-Interim observed value. SWNA = southwestern North America region; ERA = European Centre for Medium-Range Weather Forecasts Re-Analysis.

If the point is attributed to the lower (upper) quintile category, the corresponding odds ratio is plotted in blue (red). For this particular analysis no bias adjustment is needed because the quintile thresholds are computed from the hindcast.

The odds for January are similar for the three configurations. All of them display increased probabilities of lower quintile winds in North America, although they are more marked in the INI and TROP simulations. This implies that a large part of the anomaly signal was already present in the atmospheric initial conditions, regardless of the SSTs that have been used, as found in Bellprat et al. (2016). Therefore, the strong impact of the initialization in January does not allow to extract conclusions regarding the SST forcings. However, in February and March the effect of the different SSTs starts to emerge and the odds behave differently in each configuration. In February and March the odds for the INI simulation indicate that there exist increased probabilities of low wind speeds under this setting, which are consistent with the anomalies that were observed. Only a spot around 40°N and 120°W indicates enhanced probabilities of upper-quintile winds, in contradiction to what was observed. This might follow from biases in the exact location of pressure systems, which can appear in coarse-resolution configurations of EC-Earth or from the lack of ocean-atmosphere coupling in the experiments. Also, the odds and the anomalies do not necessarily need to match in all places. Internal atmospheric variability also plays a role, and therefore observed anomalies can deviate from the pattern with more probability to occur. Looking now at the CLIMSST simulation, the signal is reversed in February and March, and there is increased probability of winds above upper quintile (i.e., increased probability of high wind speeds). Therefore, without the observed SSTs that were prescribed in the INI simulation the wind anomalies would have been unlikely and we can affirm that SSTs contributed decisively to shape the event.

We have hypothesized in section 3 that NPM-related tropical Pacific SST anomalies observed in 2015 are responsible for imparting the wind speed anomalies recorded in North America, even if standardized anomalies were higher in the extratropical Pacific for this episode. The odds of the TROP simulation support this idea. Although climatological SSTs have been used in the extratropics, the obtained patterns resemble very much the INI simulation. This confirms the tropical roots of the episode. However, the odd ratio values for TROP are smaller than for INI in North America, specially during March. This indicates that the extratropical SST anomalies might have also contributed partially to maintain the event. The extratropical surface wind speed signal shows a clear Rossby wave response in the INI simulation, which is still visible in the TROP simulation. This suggests that the western tropical Pacific SSTs exert a quasi-stationary Rossby wave as discussed in Hartmann (2014) and illustrated in Trenberth et al. (1998). This has been confirmed analyzing geopotential heights at 200 hPa (Figure 9). The convective processes in WTP region (see supporting information Figure S3) produce diabatic heating in the midtroposphere and result in flow divergence and high pressures at 200 hPa level. In the INI and TROP simulations a Gill-type response to the anomalous SSTs can bee seen in the western

Pacific, similar to the Gill-type responses associated to ENSO events (DeWeaver & Nigam, 2002; García-Serrano et al., 2017). Therefore, we conclude that the physical mechanism that forced the event is similar to the mechanism at play during strong positive ENSO phases but located more to the west.

Finally, an analysis of the mean wind speed over SWNA for the three configurations has been made. In this case we use bias-adjusted data (see section 2), which allows comparison to ERA-Interim values. Figure 10 shows the probability distribution functions for wind speed averages over SWNA (only land points), drawn from the 100 ensemble members in each configuration. In February and March the distributions for INI and TROP simulations are shifted to lower wind speeds, therefore making the wind drought more probable. A Kolmogorov-Smirnov test confirms that those distributions differ significantly from CLIMSST distribution at 99% level. For March, when the episode was at its maximum, the observed anomaly was quite extreme even for the INI simulation and could not have been possible under climatological SST conditions. Analyzing the whole Q1 period, such a persistent low wind speed episode would have a return period of around 694 years according to ERA-Interim observations. But under the specific SSTs that were observed the return period descended to 48 years, making the event 14 times more probable (see supporting information Figure S4 for average Q1 distributions).

5. Discussion and Conclusions

It has been shown that the U.S. wind drought of Q1 2015 can be attributed to the North Pacific Mode state — and more specifically to its western tropical pacific anomalies — and holds no relationship with ENSO, although historically ENSO has dominated the interannual variability of wind speeds in North America. First an EOF analysis of wind speed over North America revealed that the second mode of variability was in a strongly negative phase during the first quarter of 2015, with drastic reductions of wind speed in the SWNA region. Similarly, an EOF analysis of tropical and North Pacific SSTs showed that at the same time the second variability mode (NPM) was in a very positive phase, with anomalously high SSTs off the North American shores and also in the western tropical Pacific. A relationship between those variability modes has been found in the observational records of the recent past (1979–2016), with a correlation of −0.39. The analysis suggests that western tropical Pacific anomalies associated to NPM state induce an atmospheric-bridge process and cause the wind speed reductions in the United States. Indeed, the SSTs in this area correlate to −0.56 with the second mode of wind speed. In a similar way it is found that the first wind speed mode correlates to −0.55 with NINO3.4 region SSTs (i.e., with ENSO phases).

A set of AGCM experiments has been produced for the Q1 2015 period to be able to understand causality relationships between Pacific SSTs and North American wind speeds. In a first AGCM experiment, a comparison of 100 ensemble members forced with observed anomalous SSTs and 100 ensemble members that used climatological SST averages revealed that such reductions of wind speed in SWNA were only possible under anomalous SST conditions. Therefore, SSTs are the main drivers for the observed wind speed anomalies.

A second experiment where the observed SSTs were only forced in the tropics confirmed that the extratropical wind speed anomalies arose from the tropical SST anomalies. The NPM-related extratropical SST anomalies contributed to the wind speed reductions to a lesser extent. The extratropical wind speed anomalies are linked to a Rossby wave train exerted by the warm western tropical SST anomalies which induce a wave-like response in the surface winds as shown in Figure 9. The SFM (Vimont et al., 2003) and AO (Chen et al., 2013) could also have played a role in the episode, but it has not been studied here. Also, the continuation of the episode during the second quarter of the year has not been explored.

Regarding the impact that such low wind speed episodes have in the renewable energy industry, it is clear from this study that not only ENSO events have to be tracked to anticipate wind droughts in the United States and North America, but also NPM status or other episodes of high SST in WTP are relevant. ENSO events will impart anomalies in the center and north of the continent, while NPM events will be impacting the southwest. This knowledge can be useful in the future for practical applications in the wind industry. Informing with some anticipation of probabilities of low wind speed conditions can help stakeholders to trigger some resilience mechanisms. Also, showing practical examples of how much climate oscillations can impact wind power generation will increase awareness of the need of a climate-informed wind resource assessment.

Acknowledgments
This work was funded by the EU projects S2S4E (GA 776787), EUCP (GA 776613), CLIM4ENERGY (C3S_441_Lot2_CEA), EUCLEIA (GA 607085), INDECIS (GA 690462), and MEDSCOPE (GA 690462). Omar Bellprat has been funded by the European Space Agency (ESA) Living Planet Fellowship Programme under the project VERITAS-CCI. We thank Daniel Cabezón for helping and informing on the wind drought episode and Javier García-Serrano for the insights on the interpretation of the physical processes. All the analyses have been performed using the statistical software R (R Core Team, 2015). The startR and s2dverification R packages have been used to read data sets, compute EOFs, and plot maps. Model output from the numerical experiments can be accessed through EUDAT facilities at the link http://doi.org/10.23728/b2share.71078a8618414e9b906cfa6bb7d2cdab. The reanalysis data and models used are listed in the references. We also acknowledge Javier Vegas and Nicolau Manubens for technical support, as well as the EC-Earth consortium for the model development.

References

Alexander, M. A., Bladé, I., Newman, M., Lanzante, J. R., Lau, N. C., & Scott, J. D. (2002). The atmospheric bridge: The influence of ENSO teleconnections on air-sea interaction over the global oceans. *Journal of Climate*, *15*(16), 2205–2231. https://doi.org/10.1175/1520-0442(2002)015<2205:TABTIO>2.0.CO;2

Alexander, M. A., Vimont, D. J., Chang, P., & Scott, J. D. (2010). The impact of extratropical atmospheric variability on ENSO: Testing the seasonal footprinting mechanism using coupled model experiments. *Journal of Climate*, *23*(11), 2885–2901. https://doi.org/10.1175/2010JCLI3205.1

Baxter, S., & Nigam, S. (2015). Key role of the North Pacific oscillation-West Pacific pattern in generating the extreme 2013/14 North American Winter. *Journal of Climate*, *28*(20), 8109–8117. https://doi.org/10.1175/JCLI-D-14-00726.1

Bellprat, O., Massonnet, F., García-Serrano, J., Fučkar, N. S., Guemas, V., & Doblas-Reyes, F. J. (2016). 8. The role of Arctic sea ice and sea surface temperatures on the cold 2015 February over North America. *Bulletin of the American Meteorological Society*, *97*(12), S36–S41. https://doi.org/10.1175/BAMS-D-16-0159.1

Bond, N. A., Cronin, M. F., Freeland, H., & Mantua, N. (2015). Causes and impacts of the 2014 warm anomaly in the NE Pacific. *Geophysical Research Letters*, *42*, 3414–3420. https://doi.org/10.1002/2015GL063306

Brower, M. (2015). The North American 'wind drought': Is it the new normal?, AWS Truepower. 9 December 2015. Retrieved from https://www.awstruepower.com/the-north-american-wind-drought/. (Last accessed: 31 July 2017).

Buizza, R., & Palmer, T. N. (1995). The singular-vector structure of the atmospheric global circulation. *Journal of the Atmospheric Sciences*, *52*(9), 1434–1456. https://doi.org/10.1175/1520-0469(1995)052<1434:TSVSOT>2.0.CO;2

Cayan, D. R. (1992). Latent and sensible heat flux anomalies over the northern oceans: Driving the sea surface temperature. *Journal of Physical Oceanography*, *22*(8), 859–881. https://doi.org/10.1175/1520-0485(1992)022<0859:lashfa>2.0.co;2

Chen, S., Chen, W., Yu, B., & Graf, H. F. (2013). Modulation of the seasonal footprinting mechanism by the boreal spring Arctic Oscillation. *Geophysical Research Letters*, *40*, 6384–6389. https://doi.org/10.1002/2013GL058628

Climate Prediction Center and International Research Institute for Climate and Society (2014). El Niño/Southern Oscillation (ENSO) diagnostic discussion. Retrieved from https://www.cpc.ncep.noaa.gov/products/analysis_monitoring/enso_disc_jul2014/ensodisc.html (Last accessed: 7 August 2017).

Dee, D. P., Uppala, S. M., Simmons, A. J., Berrisford, P., Poli, P., Kobayashi, S., et al. (2011). The ERA-Interim reanalysis: Configuration and performance of the data assimilation system. *Quarterly Journal of the Royal Meteorological Society*, *137*(656), 553–597. https://doi.org/10.1002/qj.828

Deser, C., & Blackmon, M. L. (1995). On the relationship between tropical and North Pacific sea surface temperature variations. *Journal of Climate*, *8*(6), 1677–1680. https://doi.org/10.1175/1520-0442(1995)008<1677:OTRBTA>2.0.CO;2

DeWeaver, E., & Nigam, S. (2002). Linearity in ENSO's atmospheric response. *Journal of Climate*, *15*(17), 2446–2461. https://doi.org/10.1175/1520-0442(2002)015<2446:LIESAR>2.0.CO;2

Di Lorenzo, E., Cobb, K. M., Furtado, J. C., Schneider, N., Anderson, B. T., Bracco, A., et al. (2010). Central Pacific El Niño and decadal climate change in the North Pacific Ocean. *Nature Geoscience*, *3*(11), 762–765. https://doi.org/10.1038/ngeo984

Ding, R., Li, J., Tseng, Y.-H., Sun, C., & Guo, Y. (2015). The Victoria mode in the North Pacific linking extratropical sea level pressure variations to ENSO. *Journal of Geophysical Research: Atmospheres*, *120*, 27–45. https://doi.org/10.1002/2014JD022221

ESS-BSC Catalogue, Earth System Services, Earth Science Department, Barcelona Supercomputing Center (2016). ERA-Interim seasonal Niño 3.4 impact on 10 m wind speed and 2 m temperature. Retrieved from http://www.bsc.es/ess/content/era-interim-seasonal-ni%C3%B1o-34-impact-10m-wind-speed-and-2m-temperature (Last accessed: 20 October 2017).

García-Serrano, J., Cassou, C., Douville, H., Giannini, A., & Doblas-Reyes, F. J. (2017). Revisiting the ENSO teleconnection to the tropical North Atlantic. *Journal of Climate*, *30*(17), 6945–6957. https://doi.org/10.1175/JCLI-D-16-0641.1

Global Wind Energy Council (2016). Global wind energy outlook 2016.

Hartmann, D. L. (2014). Pacific sea surface temperature and the winter of 2014. *Geophysical Research Letters*, *42*, 1894–1902. https://doi.org/10.1002/2015GL063083.Received

Hazeleger, W., Wang, X., Severijns, C., Ştefănescu, S., Bintanja, R., Sterl, A., et al. (2012). EC-Earth v2.2: Description and validation of a new seamless Earth system prediction model. *Climate Dynamics*, *39*(11), 2611–2629. https://doi.org/10.1007/s00382-011-1228-5

Horel, J. D., & Wallace, J. M. (1981). Planetary-scale atmospheric phenomena associated with the Southern Oscillation. *Monthly Weather Review*, *109*(4), 813–829. https://doi.org/10.1175/1520-0493(1981)109<0813:PSAPAW>2.0.CO;2

Mantua, N. J., Hare, S. R., Zhang, Y., Wallace, J. M., & Francis, R. C. (1997). A Pacific interdecadal climate oscillation with impacts on salmon production. *Bulletin of the American Meteorological Society*, *78*(6), 1069–1079. https://doi.org/10.1175/1520-0477(1997)078<1069:APICOW>2.0.CO;2

Manubens-Gil, D., Vegas-Regidor, J., Prodhomme, C., Mula-Valls, O., & Doblas-Reyes, F. J. (2016). Seamless management of ensemble climate prediction experiments on HPC platforms. In *2016 International Conference on High Performance Computing & Simulation (HPCS)* (pp. 895–900). Innsbruck, Austria: IEEE. https://doi.org/10.1109/HPCSim.2016.7568429

Maverick, T. (2015). El niño buffers U.S. wind power dreams, Wall Street Daily. 21 September 2015. Retrieved from https://www.wallstreetdaily.com/2015/09/21/u-s-wind-power-el-nino/. (Last accessed: 31 July 2017).

Meyer, G. (2015). US clean energy suffers from lack of wind, Financial Times. 1 September 2015. Retrieved from https://www.ft.com/content/b967b6d4-5058-11e5-8642-453585f2cfcd. (Last accessed: 31 July 2017).

Monahan, A. H., & Dai, A. (2004). The spatial and temporal structure of ENSO nonlinearity. *Journal of Climate*, *17*(15), 3026–3036. https://doi.org/10.1175/1520-0442(2004)017<3026:TSATSO>2.0.CO;2

North, G. R., Bell, T. L., Cahalan, R. F., & Moeng, F. J. (1982). Sampling errors in the estimation of empirical orthogonal functions. *Monthly Weather Review*, *110*(7), 699–706. https://doi.org/10.1175/1520-0493(1982)110<0699:SEITEO>2.0.CO;2

Obama, B. (2017). The irreversible momentum of clean energy. *Science*, *355*(6321), 126–129. https://doi.org/10.1126/science.aam6284

Pegion, K., & Alexander, M. (2013). The seasonal footprinting mechanism in CFSv2: Simulation and impact on ENSO prediction. *Climate Dynamics*, *41*(5-6), 1671–1683. https://doi.org/10.1007/s00382-013-1887-5

Prodhomme, C., Batté, L., Massonnet, F., Davini, P., Bellprat, P., Guemas, V., & Doblas-Reyes, F. J. (2016). Benefits of increasing the model resolution for the seasonal forecast quality in EC-Earth. *Journal of Climate*, *29*(24), 9141–9162. https://doi.org/10.1175/JCLI-D-16-0117.1

Prodhomme, C., Doblas-Reyes, F., Bellprat, O., & Dutra, E. (2016). Impact of land-surface initialization on sub-seasonal to seasonal forecasts over Europe. *Climate Dynamics*, *47*(3-4), 919–935. https://doi.org/10.1007/s00382-015-2879-4

R Core Team (2015). *R: A language and environment for statistical computing*. Vienna, Austria: R Foundation for Statistical Computing.

Seager, R., Hoerling, M., Schubert, S., Wang, H., Lyon, B., Kumar, A., et al. (2015). Causes of the 2011–14 California drought. *Journal of Climate*, *28*(18), 6997–7024. https://doi.org/10.1175/JCLI-D-14-00860.1

St. George, S., & Wolfe, S. A. (2009). El niño stills winter winds across the southern Canadian prairies. *Geophysical Research Letters*, *36*, L23806. https://doi.org/10.1029/2009GL041282

Stuecker, M. F. (2018). Revisiting the Pacific Meridional Mode. *Scientific Reports*, *8*(1), 3216. https://doi.org/10.1038/s41598-018-21537-0

Torralba, V., Doblas-Reyes, F. J., MacLeod, D., Christel, I., & Davis, M. (2017). Seasonal climate prediction: A new source of information for the management of wind energy resources. *Journal of Applied Meteorology and Climatology*, *56*(5), 1231–1247. https://doi.org/10.1175/JAMC-D-16-0204.1

Trenberth, K. E. (1997). The definition of El Niño. *Bulletin of the American Meteorological Society*, *78*(12), 2771–2777. https://doi.org/10.1175/1520-0477(1997)078<2771:TDOENO>2.0.CO;2

Trenberth, K. E., Branstator, G. W., Karoly, D., Kumar, A., Lau, N.-C., & Ropelewski, C. (1998). Progress during TOGA in understanding and modeling global teleconnections associated with tropical sea surface temperatures. *Journal of Geophysical Research*, *103*(C7), 14,291–14,324. https://doi.org/10.1029/97JC01444

U.S. Energy Information Administration (2017). Electric power monthly, with data for May 2017.

Vimont, D. J., Wallace, J. M., & Battisti, D. S. (2003). The seasonal footprinting mechanism in the Pacific: Implications for ENSO. *Journal of Climate*, *16*(16), 2668–2675. https://doi.org/10.1175/1520-0442(2003)016<2668:TSFMIT>2.0.CO;2

Wang, S.-Y., L'Heureux, M., & Chia, H.-H. (2012). ENSO prediction one year in advance using western North Pacific sea surface temperatures. *Geophysical Research Letters*, *39*, L05702. https://doi.org/10.1029/2012GL050909

Wilks, D. S. (2005). *Statistical methods in the atmospheric sciences* (2nd ed., Vol. 100). Boston: International Geophysics, Academic Press.

Yu, J. Y., & Paek, H. (2015). Precursors of ENSO beyond the tropical Pacific. *Clivar Variations*, *13*(1), 15–20.